Journal of The
Electrochemical Society

Closing the Hydrogen and Oxygen Mass Balance for PEM Water Electrolysis

To cite this article: Anna T. S. Freiberg and Simon Thiele 2025 *J. Electrochem. Soc.* **172** 034506

Journal of The Electrochemical Society, 2025 **172** 034506

Closing the Hydrogen and Oxygen Mass Balance for PEM Water Electrolysis

Anna T. S. Freiberg[1,2,z] **and Simon Thiele**[1,2]

[1]*Helmholtz-Institute Erlangen-Nürnberg for Renewable Energy (IET-2), Forschungszentrum Jülich, Cauerstr. 1, 91058 Erlangen, Germany*
[2]*Department of Chemical and Biological Engineering, Friedrich-Alexander-Universität Erlangen-Nürnberg, Cauerstr. 1, 91058 Erlangen, Germany*

In this study we show the possibility to close the hydrogen and oxygen mass balance for proton exchange membrane (PEM) water electrolysis cells at lab scale at 80 °C. By a combined analysis of the cathode and anode exhaust with respect to the absolute hydrogen and oxygen gas fluxes detected, we can quantify the true Faradaic efficiency of the system with respect to hydrogen production. While both exhausts, anode and cathode, contain an apparent hydrogen flux, there is a certain missing hydrogen share not leaving the cell, corresponding to roughly 2% at ambient pressure operation. This missing hydrogen flux shows a 2:1 correlation with the missing oxygen flux determined from the oxygen mass balance, proving that the inefficiency stems from a cell internal process. We observe a linear correlation of missing hydrogen flux with current density for different operating pressure cases, hinting toward an oxygen crossover based hydrogen loss at the cathode. The effect of the true Faradaic efficiency on the overall production efficiency of the single cells at atmospheric pressure as well as differential and balanced elevated pressure of 10 bar_a is shown, revealing a very limited operation window for efficient hydrogen production.
 [DOI: 10.1149/1945-7111/adb7c8]

Manuscript submitted January 1, 2025; revised manuscript received February 9, 2025. Published March 12, 2025.

Proton exchange membrane water electrolysis (PEMWE) is ought to play a crucial role in the future decarbonization of major energy sectors.[1,2] The possibility to store inherently fluctuating renewable energy by wind and solar in the form of chemical energy, i.e., hydrogen gas, is the main motivation to advance this technology, which is already partially in application.[3] However, the costs for producing hydrogen via this technology are still debated.[4–7]

A major driver for the cost of hydrogen produced by PEMWE is the large investment cost caused by the necessity to work with noble metals as electrocatalysts, namely platinum for the hydrogen evolution reaction (HER) and iridium-based catalysts for the oxygen evolution reaction (OER). Especially the scarcity of iridium and the currently still needed large areal loadings in order to allow hydrogen production with low electrical energy cost (i.e., at low overpotentials) are problematic for large-scale application of the PEMWE technology.

Reducing the necessary amount of iridium to lower the cost of hydrogen production is probably the key challenge current research is focusing on. However, there are other aspects that have to be considered when thinking about the applicability of PEMWE. One important aspect that has already been the focus of many studies is the hydrogen crossover phenomenon. Hydrogen is commonly found in PEMWE cells at the anode exhaust, especially when working with thin membranes—which improve the electrical efficiency of the system by reducing the ohmic overpotential—or when working at elevated cathode pressures. The latter would be beneficial because hydrogen is commonly stored at high pressure in suited vessels and mechanical compression of hydrogen is an energy intensive process.

Though this crossover phenomenon necessarily leads to a loss in efficiency of the system, it is debated mainly from a safety point of view. The explosive regime of hydrogen in oxygen ranges from 4%–95%$_{vol}$.[8] For systems to be operated safely, usually a maximum tolerable amount corresponding to 50% of the lower explosive limit (LEL) is set. While oxygen crossing over to the hydrogen side is expected to be chemically recombined with the hydrogen present on the platinum-based cathode catalyst, there is a significant hydrogen content measureable in the anode exhaust. In general, the hydrogen oxidation reaction (HOR) activity of the iridium-based anode catalyst at the high anodic potentials during OER has been considered negligible in former studies.[9,10]

For the hydrogen crossover, a diffusion-limited permeation mechanism has been discussed in literature. The hydrogen at the cathode is dissolving into the proton exchange membrane, diffusing through the bulk of the membrane and is then transitioning from the electrolyte/anode interface into the anode compartment. This mechanism is nicely observed for *in situ* permeation measurements when the electrolyte membrane thickness is varied, with the flux of hydrogen observed in the anode decreasing linearly with the membrane thickness increase.[10–12] At this point we want to emphasize that the term permeation is used herein for a mass transfer mechanism over the PEM based on solubility, diffusivity and volatility, i.e., with a pure diffusive mass transport through the PEM. However, for measurements under operation (i.e., at significant current densities) the hydrogen flux to the anode compartment at ambient pressure is increasing, easily reaching an order of magnitude higher values than what would be expected from *in situ* permeation measurements. Though several hypotheses have been stated so far, a mechanistic understanding of this behavior is still missing. Most commonly the increased permeation is ascribed to an increase of hydrogen activity close to the membrane either by (i) a net local pressure increase (due to the evolution rate exceeding the threshold for efficient gas removal via the gas diffusion layer without local overpressure at the catalyst layer-membrane interface) or (ii) by a local concentration increase significantly exceeding the steady-state saturation pressure of hydrogen, i.e., the oversaturation effect.

In order to prevent the formation of explosive mixtures at the anode, the addition of a recombination catalyst has been studied. With platinum being the catalyst of choice, several locations in the PEMWE system have been discussed.[13–15] External recombiners (i.e., after the cell) can be inserted into the exhaust stream of the PEMWE anode, though there remains a certain volume of possible explosive mixtures between the recombiner and the anode compartment. Within the PEMWE cell, addition of recombination catalysts into the anode catalyst layer[16] or onto the PTL have been studied. The latter is mainly motivated by the decrease in contact resistance from the PTL to the anode catalyst layer when adding a precious metal to the porous titanium structure,[15,17,18] but a decrease in hydrogen crossover in the anode exhaust has been observed concurrently.[15,19]

[z]E-mail: a.freiberg@fz-juelich.de

While it is hard to differentiate between a recombination mechanism (forming water as product) and an HOR mechanism (forming protons and electrons) within the anode electrical components, the addition of platinum to the membrane has been shown to decrease the crossover hydrogen flux by a recombination mechanism with oxygen.[20–23] The exact location, platinum particle size, platinum dispersion and of course platinum amount will all play a role in the effectiveness of this recombination layer. Additionally, it has been shown that membrane degradation can be aggravated due to the addition of such layers.[24] The long-term stability and activity of such cell-internal recombination catalysts is still to be proven.

Besides the safety concern, the efficiency aspect regarding product loss caused by gas crossover deserves further attention and is so far hardly studied. Hydrogen found at the anode exhaust is an apparent loss regarding the Faradaic efficiency of the system toward hydrogen. Oxygen crossing over to the cathode side will lead to an additional Faradaic loss caused by the consumption of two moles of hydrogen for each mole of oxygen reacting on the platinum surface. The oxygen crossover can therewith have a substantial impact on the overall efficiency of the system.

Due to the fast recombination on the cathode catalyst, however, it is hard to quantify the amount of oxygen crossing over experimentally. In most former crossover studies the oxygen crossover was commonly neglected[10,25–27] or only taken into account assuming a pure permeation mechanism.[20,23] Trinke et al.[28] have tried to replace the platinum-based cathode catalyst with a non-noble metal catalyst. They could show that the amount of oxygen in the cathode is actually substantial, and it is significantly exceeding a simple oxygen permeation mechanism. However, as the catalyst chosen is unknown, it remains unclear whether the amount of oxygen detected in the cathode exhaust is really representative of the overall amount of oxygen that crosses over.

In this study we aim to close the hydrogen mass balance and report the actual hydrogen production efficiency by taking into account the real Faradaic efficiency and the electrical efficiency.

In a custom made test station we are able to do composition and absolute flux analysis of both single cell exhaust streams using a mass spectrometer. By variation of the operating pressure we show how the gas fluxes change for different operation strategies and end up with a cell-based hydrogen production efficiency that shows the importance of actual product stream analysis on efficiency values, which was so far not done in literature. We have chosen the most basic MEA and cell configuration in order to provide fundamental insights.

Experimental

Gas balance analysis and efficiency calculation.—As explained in the introduction, the gas balance within PEMWE is complex and different assumptions have been made in literature to estimate the Faradaic efficiency for hydrogen production $\eta_{H_2}^{FA}$, which is generally defined as

$$\eta_{H_2}^{FA} = 2 \cdot \frac{N_{H_2}^{cath}}{N_{e^-}} = 2 \cdot \frac{N_{H_2}^{cath} \cdot F}{I} \qquad [1]$$

with $N_{H_2}^{cath}$ being the actual hydrogen mole flux found at the cathode exhaust, F being the Faraday constant and I the absolute current supplied to the PEMWE cell. $\eta_{H_2}^{FA}$ can differ from unity by taking into account all possible parasitic mole fluxes stemming from imperfect material and system properties as depicted in Fig. 1. In an ideal case (left scenario in Fig. 1), $\eta_{H_2}^{FA}$ can be calculated directly from measuring the amount of hydrogen leaving the anode $N_{H_2}^{an}$, which is equal to the crossover hydrogen flux $N_{H_2}^{cross}$. At this point it has to be noted that the measurement principle, i.e., whether the absolute flux $N_{H_2}^{an}$ is measured via gas chromatography or mass spectrometer or whether the H_2 in O_2 content is measured can lead to slightly different values due to a finite oxygen loss via the membrane $N_{O_2}^{cross}$ as shown later in Fig. 7.

Oxygen crossing over to the cathode side $N_{O_2}^{cross}$ will lead to an additional Faradaic loss. Assuming most of the oxygen reaching the cathode to recombine (middle scenario in Fig. 1), we can therewith rewrite Eq. 1 to

$$\begin{aligned}\eta_{H_2}^{FA} &= 2 \cdot \frac{\frac{1}{2}N_{e^-} - N_{H_2}^{cross} - 2 \cdot N_{O_2}^{cross}}{N_{e^-}} = 1 - \frac{2 \cdot N_{H_2}^{cross}}{N_{e^-}} - \frac{4 \cdot N_{O_2}^{cross}}{N_{e^-}} \\ &= 1 - (X_{H_2}^{cross} + 2 \cdot X_{O_2}^{cross}) \end{aligned} \qquad [2]$$

with $N_{H_2}^{cross}$ being the hydrogen flux reaching the anode, $N_{O_2}^{cross}$ being the oxygen flux reaching the cathode and X^{cross} representing the respective molar share of the gas crossing over the membrane. For the full balance used within this manuscript (right hand side of Fig. 1) we do not assume the amount of crossover oxygen $N_{O_2}^{cross}$ to be negligible. Additionally we do not want to postulate the HOR activity of the anode to be negligible. We call the flux of hydrogen detected at the anode $N_{H_2}^{an}$ an apparent hydrogen crossover, that only

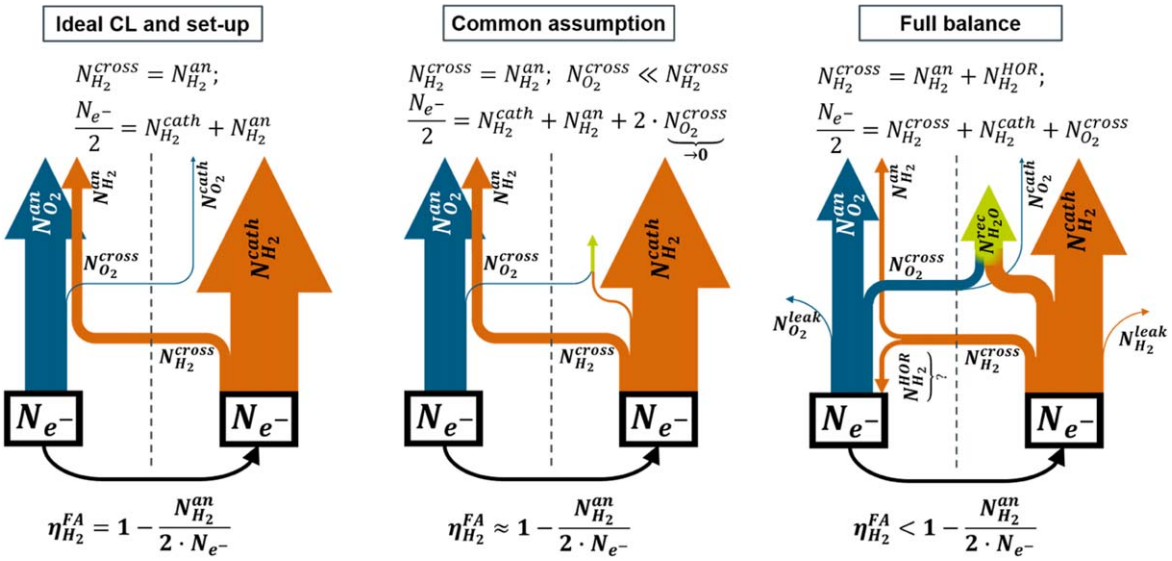

Figure 1. Gas fluxes considered for efficiency calculations with increasing complexity from left to right denoted as Sankey diagrams. The dashed vertical line shall represent the separation of the anode and the cathode.

serves as a lower limit estimate of the absolute amount of hydrogen leaving the cathode compartment via the PEM, $N_{H_2}^{cross}$. In general also the gas leakage of the set-up resulting in additional losses denoted as N^{leak} in Fig. 1 must be considered.

We quantify the Faradaic efficiency based on Eq. 1 and additionally report the directly measureable values of $N_{H_2}^{cath}$, $N_{H_2}^{an}$, $N_{O_2}^{an}$ and $N_{O_2}^{cath}$. Comparing those values to the theoretically produced fluxes of hydrogen and oxygen based on Faraday's Law ($z = 2$ for the hydrogen mass balance, $z = 4$ for the oxygen mass balance), we quantify the amount of missing product gases $N^{missing}$ according to Eq. 3.

$$N^{missing} = \frac{N_{e^-}}{z} - (N^{cath} + N^{an}) = \frac{I}{F \cdot z} - (N^{cath} + N^{an}) \quad [3]$$

Looking at the right hand scheme in Fig. 1 we can sum up the fluxes going into the parasitic loss terms for hydrogen and oxygen resulting in Eqs. 4.1 and 4.2.

$$N_{H_2}^{missing} = N_{H_2}^{HOR} + N_{H_2}^{leak} + 2 \cdot (N_{O_2}^{cross} - N_{O_2}^{cath}) \quad [4.1]$$

$$N_{O_2}^{missing} = \frac{1}{2} N_{H_2}^{HOR} + N_{O_2}^{leak} + (N_{O_2}^{cross} - N_{O_2}^{cath}) \quad [4.2]$$

For a set-up where the leak rates are negligible, the amount of missing hydrogen and missing oxygen will therewith follow a 2:1 ratio.

The electrical efficiency $\eta_{H_2}^{EC}$ is defined as

$$\eta_{H_2}^{EC} = \frac{E_{LHV}}{E_{cell}} = \left| \frac{-\Delta H^0}{2 \cdot F \cdot E_{cell}} \right| \quad [5]$$

with E_{LHV} representing the minimum potential based on the lower heating value of hydrogen and ΔH^0 the reaction enthalpy for water in its gaseous state $\left(\Delta H^0 = -242 \frac{kJ}{mol} \rightarrow E_{LHV} = 1.25V\right)$.

The hydrogen production efficiency can therewith be calculated according to Eq. 6.

$$\eta_{H_2}^{Prod.} = \eta_{H_2}^{EC} \cdot \eta_{H_2}^{FA} \quad [6]$$

MEA preparation.—The 5 cm^2 active area MEAs used throughout this study were prepared by a standard decal transfer method. For the anode ink, the commercial iridium oxide/titanium dioxide anode catalyst powder (Elyst Ir75 0480, Umicore, 74.6%$_{wt}$ iridium) was mixed with a 20%$_{wt}$ ionomer dispersion (D2021, Chemours), DI water and 2-propanol (Sigma Aldrich, > 99.9% purity). The ink had a total catalyst content of 46%$_{wt}$, an ionomer solid content of 11.6%$_{wt}$ and a solvent ratio of roughly 1%$_{wt}$ H_2O in 2-propanol (excluding the ionomer dispersion). A 5 ml ink batch was mixed in a 16 ml HDPE bottle with 33 ZrO_2 beads (5 mm_{dia}, Fritsch, Germany) on a roller mill at 180 rpm for 20 h. The ink was spread on a 50 μm virgin PTFE substrate with a 80 μm wetfilm thickness Mayer-Rod at 10 mm s^{-1}. The coating was left for drying first at room temperature until visually dry (< 30 min). Then the coating was placed in a convection oven at 70 °C for 3 h. 5 cm^2 active area electrodes were cut using a stencil in square shape. The dry thickness of the anode coatings was 11 ± 1 μm and the loading of the electrodes was $2.02 \pm 0.12 \frac{mg_{Ir}}{cm^2}$.

The cathode electrodes were fabricated similarly with minor parameter adjustments as stated. The commercial platinum on carbon catalyst powder (Pt50 0380, Umicore, 50%$_{wt}$ Pt) was mixed with a 20%$_{wt}$ ionomer dispersion (D2021, Chemours), DI water and 1-propanol (Sigma Aldrich, > 99.9% purity). The ink had a total catalyst content of 13%$_{wt}$, an ionomer to carbon ratio of 0.65 and roughly 4%$_{wt}$ H_2O in 1-propanol (excluding the ionomer dispersion). A 5 ml ink batch was mixed in a 16 ml HDPE bottle with 33 ZrO_2 beads (5 mm_{dia}, Fritsch, Germany) on a roller mill at 60 rpm for 20 h. The ink was spread on a 50 μm virgin PTFE substrate with a 100 μm wetfilm thickness Mayer-Rod at 10 mm s^{-1}. The dry thickness of the cathode coatings was 6 ± 1 μm and the loading of the electrodes was $0.23 \pm 0.01 \frac{mg_{Pt}}{cm^2}$.

Both electrodes were hot-pressed onto a commercial Nafion™ membrane (N212, Chemours, 51 μm dry thickness, 6 cm × 6 cm) in a single hot-press step at 2.5 MPa, 155 °C for 6 min. Pacopads (Pacopad #5500, Pacothane Technologies, USA) were used as pressure distribution medium during the hot-pressing step. A sheet of 50 μm Kapton® was added between the electrodes and the Pacopads to prevent contamination of the MEA. The electrode loading was determined based on the cut electrode weight and the weight of the respective decal foils after hot-pressing.

Cell assembly.—The general cell design was adapted from Bernt and Gasteiger.[29] Single channel, 7 serpentine flow fields milled from grade 1 titanium with gold coating were used on anode and cathode. A sintered titanium powder PTL (Mott Corporation, USA, 50% porosity, 258 ± 5 μm) was used on the anode side and a carbon paper GDL without MPL (TGP-H-120T, Toray, Japan, 5% PTFE, 332 ± 2 μm) was used on the cathode side. The GDL and PTL were cut to dimensions of 2.6 cm × 2.6 cm. A 10 μm virgin PTFE subgasket (Goodfellow, UK) was used on the anode side and a 25 μm virgin PTFE subgasket (Hightechflon, Germany) was used on the cathode side, each with a cutout of 2.35 cm × 2.35 cm. Adjustment of the cell compression was done using the thickness of the virgin PTFE gaskets (Hightechflon, Germany), assuming a membrane swelling of 50%. The thickness of the virgin PTFE gaskets were chosen to result in a GDL nominal compression of 20 ± 2%, whereas 3% of settling of the PTFE gaskets during cell compression was accounted for. The cell was tightened with twelve M10 screws and with 15 Nm torque each, which was reached in steps of 2.5 Nm.

Electrochemical protocol for MEA testing.—Three MEAs were tested to ensure reproducibility. After cell assembly, and leak check with nitrogen gas, the cell was flushed with 20 ml min^{-1} H_2O on the anode and 200 sccm nitrogen on the cathode without backpressure. After reaching a temperature of 80 °C, the cell was left to equilibrate for 30 min. To exclude electrical shorts, a test was executed at 1.3 V cell voltage with active 100 sccm of hydrogen on the cathode with a maximum short current of 0.2 mA cm^{-2}. A simple conditioning protocol was applied afterwards: The current was ramped up at 10 mA s^{-1} to a total current of 5 A (i.e., 1 A cm^{-2}), followed by a hold for 30 min without active hydrogen supply. Three short galvanostatic polecurves with a holding time of 5 min at each current density were measured consecutively, whereas it was ensured that the cell potential never decreased below 1.3 V. After conditioning at 80 °C and ambient pressure, CVs at 50 mV s^{-1} in the range of 0.1–1.3 V were recorded to track the begin-of-test state of the anode catalyst with 100 sccm hydrogen flux on the cathode and 20 ml min^{-1} H_2O on the anode.

Afterwards the gas crossover measurements were conducted. For this, a polarization curve with 30 min holding time was recorded between 10 mA cm^{-2} and 4 A cm^{-2} at 80 °C and at symmetric ambient pressure without active hydrogen supply. The cell potential was set to 1.3 V and the cathode pressure was increased by the active hydrogen line set to 100 sccm. When a cathode pressure of 10 bar_a was reached, the hydrogen flux was decreased to 10 sccm and kept constant throughout the elevated pressure measurements. A re-conditioning at the elevated pressure was executed including the current ramp to and 30 min hold at 1 A cm^{-2} and two short polecurves with 5 min holding time per measurement point. The gas crossover measurements were conducted as described above. The same protocol was applied for the symmetric elevated pressure operation at 10 bar_a/10 bar_a.

After the crossover measurements, the cell was brought back to symmetric ambient pressure operation and the short reconditioning protocol was applied followed by end-of-test CVs.

The voltage difference between the third short polecurve during the initial conditioning and the last short polecurve after the crossover measurements was less than 0.3% for all MEAs at all current densities. Along with the overlap of the CV features at begin-of-test and end-of-test we therefore conclude that the cell has not undergone aging during the measurement sequence. Except for the four CV cycles at begin-of-test and end-of-test (each) the cell potential never dropped below 1.3 V. One MEA was additionally tested for its crossover characteristics at ambient pressure after the elevated pressure operation. The gas fluxes observed were well within the error range shown for the begin-of-test ambient pressure measurement.

For the polarization curve data shown in this study, the last 5 min of the constant current hold steps during the crossover measurement polarization curve were averaged. All polarization curves contained galvanostatic electrochemical impedance spectroscopy measurements at all current densities with an excitation in AC current corresponding to 10% of the DC load with a minimum of 3 mA cm^{-2} in the frequency range of 200 kHz to 100 mHz. The impedance data is not further discussed here but was recorded to ensure no unexpected changes especially with respect to HFR were observed throughout testing.

Test station set-up.—To directly quantify the gas composition and absolute volume flows produced in the PEMWE single cells at different operation conditions, a dedicated test station was developed. A simplified flow diagram is shown in Fig. 2. The anode of the PEMWE cell (left hand side in Fig. 2) is fed with DI water. The water is fed by a gear pump, whereas an additional digital liquid mass flow controller (MFC) is controlling the pump speed to ensure a constant feeding rate even at elevated backpressure. The DI water is pumped from a reservoir (inertized by continuous nitrogen bubbling) and passes through an ion-exchanger and a conductivity indicator (CI) before being pre-heated to enter the cell. All measurements were conducted with feed water resistivities of at least 16 MOhm cm. The water-gas mixture leaving the cell is diluted downstream with nitrogen whereas an exact volume flow of 200 sccm is ensured by a digital MFC (Bronkhorst EL-Flow Prestige; calibrated to 200 sccm of N_2 with an accuracy of ± 0.6% // ± 1.2 sccm). This nitrogen stream (5.0 grade) serves as internal reference for the mass spectrometer (MS) data as explained later. After dilution, the backpressure regulator (PC) is passed, before the anode exhaust mixture is guided into a simple drainer to separate the liquid water from the humid gas stream. The drainer is kept at elevated temperature (roughly 60 °C) to minimize the error caused by dissolved product gas in the water phase. The water is drained back into the DI water reservoir and the gas is fed into the multi-sampler head of the MS.

On the cathode side of the test station (right hand side of Fig. 2) an active hydrogen line is added to be able to preset the cathode half-cell potential and to actively pressurize the cathode up to 10 bar_a. The pressure is controlled by a digital backpressure controller directly after the cathode cell outlet. For measurements with ambient backpressure, after initially flushing the cell with active hydrogen, the flow is stopped and the solenoid valve at the cell inlet is closed. For elevated pressure operation at the cathode, a small continuous flow of 10 sccm of hydrogen (5.0 grade) was fed to the cell to ensure stable pressure operation even at OCV conditions and at small current densities where the hydrogen production rate is small. This small continuous flux was achieved by a low flow digital MFC (Bronkhorst EL-Flow Prestige; calibrated to 100 sccm of H_2 with an accuracy at 10 sccm of ± 0.15 sccm). This set hydrogen flux resulted in a background signal in the MS, which was corrected for by using the signal obtained during the 1.3 V hold at the beginning of each polarization curve. After the backpressure regulator, the gases from the cathode exhaust are diluted with 200 sccm of nitrogen just as for the anode case. After passing a drainer to prevent liquid water from reaching the MS, the humid product gases are fed into the multi-sampler head of the MS as well. Due to the large osmotic drag coefficient for PEMs, the drainer on the cathode is necessary due to liquid water formation. The liquid from the cathode drainer is discarded.

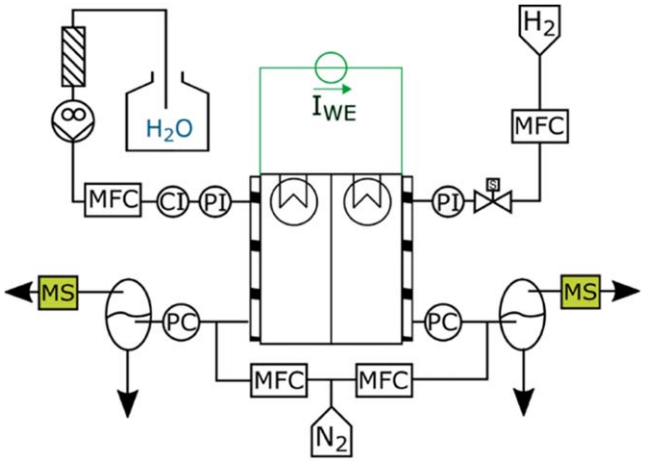

Figure 2. Simplified flow diagram of the test setup developed for the hydrogen mass balance analysis. The product gases of both, anode and cathode compartment, are diluted with 200 sccm of N_2 before being directed to a mass spectrometer.

Analysis of mass spectrometry data.—Quantification of the gases was done using a magnetic sector mass spectrometer (Prima BT, ThermoOnix Ltd, UK). In contrast to gas chromatography devices, the MS system does not rely on dry sample gases and can work up to a sample dew point of 70 °C. The MS uses a Thoria filament as ionization source, a magnetic sector analyzer and a Faraday cup detector. The MS is equipped with a multi-sampler head of up to 16 inlets, whereas a motor controls the position of the sampling head to the stream of interest. Sample streams not characterized at a given time are simply guided to the exhaust. For the chosen sample stream, a fixed amount is fed through a capillary to reach the filament. Quantification of the hydrogen, water, nitrogen and oxygen flow was done according to the signals at a mass to charge ratio (m/z) of 2, 18, 28 and 32, respectively. Though the exact water content in the gas phase is not of interest, it was needed to get exact values of the hydrogen signal as water bears a small signal fragment on $m/z = 2$ of roughly 0.05% at our MS with respect to its main signal at $m/z = 18$.

In order to quantify the absolute amount of hydrogen and oxygen gas flux on anode and cathode, the 200 sccm of N_2 added after the cell exhaust on both sides were used as an internal standard. For this, the sensitivity of the MS with respect to the quantified gases, H_2, O_2 and N_2 was calibrated using a 3/3/94 gas mixture (by volume). The data was analyzed based on the raw current signal on the corresponding channels using the calibration factor obtained from the calibration gas measurement and the given N_2 flux of 200 sccm in the exhaust gases. The pure N_2 background and the calibration gas were measured at the beginning of the measurement series of each cell and after cell shut down to correct for the baseline signal.

The multi-sampler head of the MS allows automatic alternation between the sample streams to be directed into the ionization source, analyzer and detector. The sample streams were analyzed with 5 s per data point and the sampling head was switched every 5 min between anode exhaust sample stream and cathode exhaust sample stream. The last 5 min of data from each sample stream were averaged for gas flux quantification. For the here discussed correlations, the minimum current density analyzed with respect to gas flux quantification is 50 mA cm^{-2}.

Gas flux quantity representation and set-up error estimate.— Based on the analysis of the MS data, the absolute gas flux of hydrogen and oxygen in both exhausts can be quantified. With the goal of estimating the full efficiency for hydrogen production, the gas fluxes are given as sccm/cm^2, whereas the geometric area of the electrode of 5 cm^2 was used for normalization. We represent the data as the average of independent measurements on three MEAs with the error bars denoting the min-max deviation of those.

Using the geometric area of the electrodes for normalization can lead to systematic errors with respect to the absolute crossover flux values. While the gas production according to Faraday's Law will only occur in this area, gas crossover can also happen over the rim between the electrode area and the subgasket cut-out as explained by Bernt et al.[10] In this region mass transfer between the electrode compartments is expected to run via a simple permeation mechanism without significant influence of osmotic drag and oversaturation, which is believed to be limited to the nano-porous electrode area. However, as gas crossover fluxes observed are commonly significantly higher than predictions based on simple permeation, we believe this error to be insignificant in comparison to the deviations observed between independent repetition measurements. Anyway, the Faradaic efficiency measured will still be quantitatively representative as it is based on the absolute hydrogen flux found in the cathode exhaust.

Aside of the systematic error caused by the normalization, random errors in the gathered data could stem from the measurement and analysis set-up due to insufficient device accuracies. The error of the MFCs is small as given in the explanation of the test set-up, which means that the internal nitrogen standard for absolute flux quantification will lead to minor errors in the MS sample stream (<0.6%). The non-linearity of the MS signal and leak tightness of the whole test set-up (see Fig. 2) was carefully evaluated. The PEMWE test cell was assembled with a 500 μm glass fiber reinforced gasket replacing the MEA without PTL and GDL and was connected to the test station. The liquid feed of the anode was replaced by a digital MFC (Bronkhorst EL-Flow Prestige; calibrated to 200 sccm of N_2) feeding synthetic air or the calibration gas mixture (3% H_2 and 3% O_2 in N_2). With this set-up, O_2 and H_2 product fluxes of 0.15–150 sccm were fed through the cell hardware (at ambient backpressure or 10 bar$_a$), diluted with the internal 200 sccm N_2 standard and analyzed in the MS. Over the three orders of magnitude in absolute H_2 and O_2 flux, the signal in the MS resulted in calculated values always closer to the set values than the denoted accuracy of the used MFCs. Additional errors by leakage and/or non-linearity of the MS are therefore seen to be significantly smaller than the already discussed minor error caused by the MFCs.

Additional errors of the measurements could include fluctuations in the temperature and pressure controls of the test station. As such random errors are hard to quantitatively correlate to an error in the measured gas fluxes, the usage of three independent measurements is seen to cover such errors bests.

While we only represent the gas fluxes as such without trying to quantitatively correlate them to a mass transfer based on e.g. permeation, we want to quickly point out that membrane creep might significantly influence gas permeation and other mass transfer mechanisms over the PEM. Especially when working with thin membranes and rough PTL surfaces, special attention needs to be paid to the inhomogeneous membrane creep, which most likely results in local current density distribution variations, which can affect gas crossover characteristics.

Results and Discussion

Exhaust gas quantification at ambient pressure conditions.— The capabilities of our measurement set-up to close the hydrogen mass balance even at ambient pressure and with small active cell areas of only 5 cm^2 are discussed first. For this, the exhaust gas quantities were analyzed for three individual MEAs at 80 °C, 1 bar$_a$ symmetric pressure and a water feed rate of 20 ml min^{-1}. All data shown stems from three independent measurements with the error bars representing the min-max deviation.

The first relationship we analyzed was the general dependency of the oxygen flux at the anode exhaust $N_{O_2}^{an}$ and the hydrogen flux at the cathode exhaust $N_{H_2}^{cath}$ as a function of current density (please note that the corresponding polarization data is shown and discussed in Fig. 7). In the ideal case—i.e., 100% current selectivity for OER and HER and no gas crossover—the fluxes would strictly follow Faraday's Law. As shown in Fig. 3a the general trend of Faraday's Law (green line) is of course met, but the absolute amount of hydrogen found at the cathode exhaust (orange squares) and oxygen found at the anode exhaust (blue squares) is slightly too low.

The other fluxes directly quantifiable are the apparent gas crossovers at their respective counter electrode, i.e., the hydrogen amount found in the anode exhaust $N_{H_2}^{an}$ and the oxygen content found in the cathode exhaust $N_{O_2}^{cath}$. Both are depicted in Fig. 3b as orange and blue stars, respectively. The hydrogen flux found in the anode exhaust follows the general order of magnitude and current density dependent trend as found in literature.[10,30] At current densities below 1 A cm^{-2} a small linear dependency of hydrogen flux in the anode with current density can be seen, whereas at higher current density a strong, exponential increase can be observed. The exact reason for this behavior is still strongly debated in literature and is not the focus of this study.

Hydrogen is commonly found on the anode due to the assumed low HOR activity (or recombination activity) of the iridium-based catalyst. This bears a significant safety risk due to the formation of possible explosive mixtures, which will be further discussed later in Fig. 7. Oxygen crossing over to the cathode side on the other hand is expected to undergo a fast chemical recombination on the platinum-based cathode with the hydrogen present. Still, there is a small apparent oxygen crossover in the hydrogen stream corresponding to a cathode hydrogen purity of roughly 99.98% in our measurement set-up (blue stars in Fig. 3b). This is probably caused by the limitations of the small active area cell measurements. Due to alignment purposes, the gasket cut-out is slightly larger than the active area (roughly 5.5 cm^2), which results into parts of the oxygen filled PTL structure to be in contact with the membrane with no cathode CL on the opposite side of the membrane. Therefore, oxygen can cross over without having the possibility to chemically recombine on the platinum-based catalyst. Measurements with larger cell areas will lead to a substantially lower share of oxygen impurity being present in the cathode product stream. Interestingly, the oxygen impurity seems to follow a strict linear relation with the applied current density. Comparing the flux of oxygen observed on the cathode and hydrogen found on the anode, the detectable hydrogen content is generally higher with a factor of 3 at 1 A cm^{-2} up to a factor of 7 at 4 A cm^{-2}.

Comparing the amount of hydrogen and oxygen that should have been produced according to Faraday's Law and the total amount of the respective gases found as a sum in both exhausts, there are significant amounts of product gases missing (see Eq. 3). The amounts of missing gases for the different studied current densities are shown in Fig. 3c. For a direct comparison, the amounts of the respective apparent crossover gas found on the counter electrode are added to this panel again as orange and blue stars. The first observation is that the amount of missing gases, both for the hydrogen mass balance and for the oxygen mass balance largely exceed the apparent crossover fluxes. At ambient pressure conditions, the missing amount of product gases is a factor of 5–50 larger at all current densities. An important observation is the basic fact that the amount of missing gas is strongly current density dependent. This is an implicit proof that the amounts predicted to be missing based on Faraday's Law do not stem from an insufficiently tight measurement set-up, as the latter would need to lead to a constant missing flux, independent of the current density applied. The

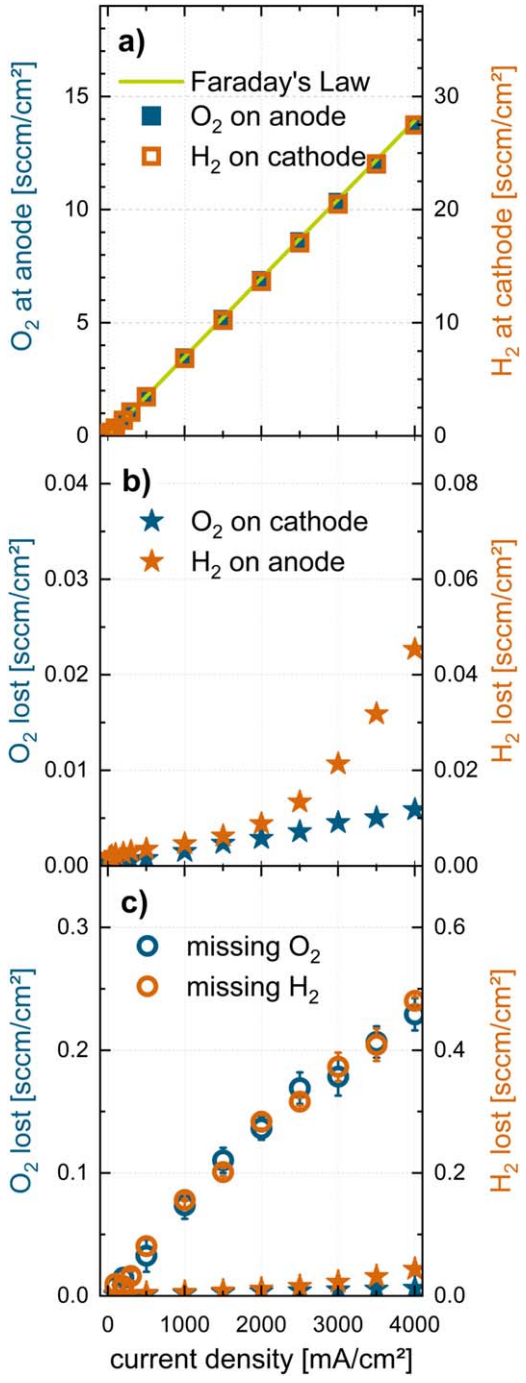

Figure 3. Quantification of gas fluxes for PEMWE cells based on a N212 membrane running at 80 °C, symmetric atmospheric pressure with 20 ml min^{-1} of H_2O supply to the anode. Three replicates were measured with the error bars corresponding to the min-max deviation. (a) Current density dependent product gas fluxes detected in their respective exhaust. H_2 flux found on the cathode ($N_{H_2}^{cath}$ orange squares, right axis) and O_2 flux found on the anode ($N_{O_2}^{an}$ blue squares, left axis) compared to the production rate according to Faraday's Law (green line). (b) Gas flux found on the opposite electrode exhaust, $N_{H_2}^{an}$ and $N_{O_2}^{cath}$. (c) Amount of missing product gas fluxes over current density $N^{missing}$ according to Eq. 3. The results of (b) (i.e., $N_{H_2}^{an}$ and $N_{O_2}^{cath}$) are added here as stars for direct comparison keeping the same color scheme.

dependency on the current density for both gases, hydrogen and oxygen follows an almost linear trend, which will be discussed in detail in conjunction with the measurements done at elevated pressure.

By plotting the oxygen and hydrogen gas fluxes in a 1:2 ratio (according to the electrochemical water splitting reaction), it becomes evident, that the information on both missing gases (though analyzed completely separately) is equipollent: There is twice as much hydrogen missing in the mass balance as oxygen. This leads to the conclusion that the analysis works out well and that the reason for the missing product gases indeed stems from a process inside of the cell rather than a leaking measurement set-up or from significant losses of the product gases through the water phase in the drainers.

In general, a product gas flux not following Faraday's Law can in the first instance mean that the selectivity of the respective half-cell reaction is not 100%, i.e., that parts of the mole flux of electrons do not participate in the desired electrochemical reaction. As the analysis was done after equilibration of 30 min at the respective current density, it must be a net reaction running that relies on continuous supply of the reactant. The electrochemical oxidation of metal components on the anode (including the catalyst) for example would be self-limiting and could by itself not lead to discrepancies in the Faradaic efficiency over longer hold times. Also the fact that both product gases, hydrogen and oxygen, show the same share of missing flux deems a general parasitic reaction to be unlikely, especially as such reaction would in the first instance only change the selectivity of one of the electrodes, not both.

However, taking into account the fact that the membrane is an imperfect barrier for gases, there are two mechanisms that could easily explain the 1:2 ratio in missing product gases. On the one hand, oxygen that is crossing over to the cathode would recombine on the platinum-based catalyst with hydrogen in a 1:2 ratio. On the other hand, hydrogen crossing over to the anode could be electrochemically oxidized to protons. Parts of the current at the anode would therewith not produce oxygen via the OER, but simply consume hydrogen via the HOR. As the cell would partially run in a simple hydrogen pumping mode, the Faradaic efficiency of both product gases would be decreased. Such an electrochemical pump can be considered a chemical short and reduces the Faradaic efficiency in the same sense as an electrical short.

The HOR activity of iridium-based catalysts (that undergo oxidation at the high anodic potentials) has been considered negligible in PEMWE permeation studies in literature.[9,10] Minding that there is still a considerable detectable amount of hydrogen gas present in the anode exhaust, this assumption seems valid. As we are starting with a rutile IrO_2 catalyst surface and throughout the measurement series ensured the potential of the cell to never drop below 1.3 V—which should prevent the reduction of the rutile phase according to Weiss et al.[31]—it might be reasonable to assume that also for our measurements the HOR activity on the anode can be neglected. However, iridium-based catalysts can change upon simple storage and are inherently unstable with respect to their surface chemistry. CVs have been recorded after conditioning and after the measurement series and did not show changes with respect to possible surface reduction. But minding the high potentials at the anode and therewith the high driving force towards HOR we consider both mechanisms for the 1:2 ratio of missing gases to be reasonable.

Effect of backpressure on missing gas quantities.—In order to differentiate between the oxygen crossover and the hydrogen crossover driven mechanisms for the 1:2 ratio of missing product gases, measurements at elevated backpressure were conducted. The same crossover measurements as for the ambient pressure case were executed at differential pressure of a 1 bar_a anode with a 10 bar_a cathode and at symmetric pressure of 10 bar_a using the same three MEAs. While the latter case is unconventional (the anode is meant to run at ambient pressure generally), it allows a simple single parameter variation to get a better understanding of the effect of oxygen crossover on the missing gas quantities.

The results of the exhaust gas quantification are shown in Fig. 4. A full discussion on the electrochemical results is done later in

Fig. 7. The hydrogen flux observed at the anode outlet $N_{H_2}^{an}$ and oxygen flux observed on the cathode outlet $N_{O_2}^{cath}$ are given as stars. The amount of missing oxygen (open blue circles) and missing hydrogen (open orange circles) are again calculated based on Eq. 3.

In Fig. 4a the gas fluxes for the differential pressure operation with 1 bar_a backpressure on the anode and 10 bar_a backpressure on the cathode are shown. While the amount of oxygen found in the cathode exhaust is still very small (blue stars), the hydrogen flux detected directly at the anode exhaust is substantial (orange stars). It does not follow the same current density dependent shape as observed for the ambient pressure case (see Fig. 3b) as it lacks the exponential increase at higher current densities. This change in apparent hydrogen crossover rate trend over current density has already been shown in literature.[10,30] Also here the exact mechanisms are not understood yet.

For the 1 bar_a/10 bar_a differential pressure operation, the missing gas amounts for oxygen and hydrogen follow a strict 1:2 correlation as well (Fig. 4a open circles). This proofs that the measurement

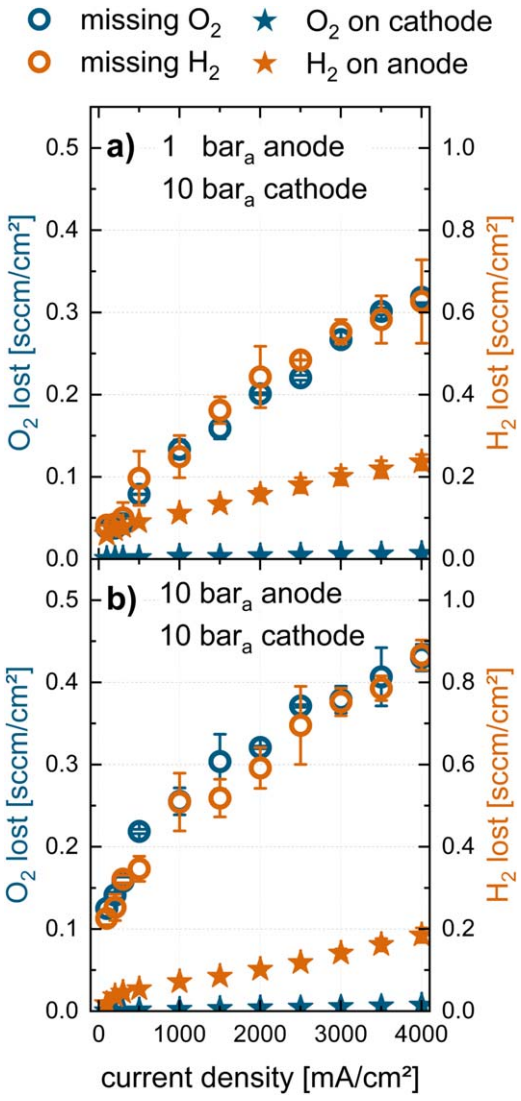

Figure 4. Quantification of gas fluxes for PEMWE cells based on a N212 membrane running at 80 °C with 20 ml min^{-1} of H_2O supply to the anode at (a) differential pressure operation at 1 bar_a/10 bar_a with elevated cathode backpressure and at (b) symmetric pressure operation at 10 bar_a/10 bar_a. Three replicates were measured with the error bars corresponding to the min-max deviation. The gas flux found on the opposite electrode exhaust is denoted as blue or orange stars. The amount of missing product gas fluxes over current density are shown as open circles.

set-up is indeed able to close the mass balances of the product gases as it does not depend on a certain set of operation parameters. While the amount of detected hydrogen on the anode is expectedly higher in case the cathode is run with 10 bar_a backpressure, interestingly also the total amount of missing hydrogen is increased, but only by a factor of roughly 1.5 at the highest current density studied of 4 A cm^{-2}. Even more so, the rather strict linear behavior of the missing gas fluxes with current density observed for the ambient pressure case is limited to the mid to high current density region.

The next logical step is to check for the dependency of the missing gas fluxes on the anode backpressure. A differential pressure measurement, however, is not possible in our set-up due to safety reasons, which is why we conducted the crossover analysis at a symmetric pressure of 10 bar_a/10 bar_a. Even with increased oxygen backpressure the amount of oxygen found in the cathode exhaust $N_{O_2}^{cath}$ is small and only 10% higher than for the ambient pressure measurements and the differential measurement at 1 bar_a/10 bar_a. As we have hypothesized that the oxygen crossing over can any way only be detected for the rim between the electrode active area and the gasket cut-out, the insignificant change of the detected oxygen in the cathode exhaust would hint toward an insignificant change in oxygen activity at the membrane interface with increasing anode back-pressure. Also, for the symmetric operation at elevated back-pressure the apparent hydrogen crossover $N_{H_2}^{an}$ is increased compared to the ambient pressure case, as expected. A deeper discussion follows in the next part.

Just as for the ambient pressure case and for the measurements executed under differential pressure, the missing amounts of oxygen and hydrogen gas found as a sum in both exhausts are following a strict 1:2 relation with both gas fluxes providing equivalent quantitative information.

Comparison of the hydrogen mass balance for different pressure conditions.—In the former chapters we have established the quantification of the oxygen and hydrogen gas fluxes to result in the same quantitative findings regarding missing amounts of product gases found in the exhausts. For an easier quantitative comparison of the mass balance, Fig. 5 shows the results obtained for the hydrogen quantification for the three discussed operating pressure settings. The left axis is showing the current lost with respect to the amount of missing hydrogen based on Faraday's Law (Fig. 5a) and for the apparent hydrogen crossover $N_{H_2}^{an}$ (Fig. 5b).

Looking at the current density dependent missing hydrogen flux, there is a strong similarity regarding the behavior at current densities exceeding 1 A cm^{-2} following a close to linear trend (taking into account the error bars stemming from the three independent MEAs analyzed). A simple linear fit with a direct weighing of the error bars at each current density was executed in the range of 0.5–4.0 A cm^{-2} and is shown as dotted lines in the respective color in Fig. 5a. All fits show a very similar slope of $0.11 - 0.13\ \frac{sccm_{H_2}}{A}$ of missing hydrogen flux. The difference in absolute values observed stems from a change in the intercept of the linear fit increasing from $0.04\ \frac{sccm_{H_2}}{cm^2}$ at symmetric atmospheric pressure (light orange) over $0.15\ \frac{sccm_{H_2}}{cm^2}$ at differential operation of 1 bar_a/10 bar_a up to $0.34\ \frac{sccm_{H_2}}{cm^2}$ at symmetric operation at 10 bar_a.

A linear dependency of the missing hydrogen gas amount whose slope over current density is independent of the operating pressure is an intriguing finding. A possible explanation for this could be for this share to be caused by oxygen crossover driven by the electro-osmotic drag as it is one of the few mass transport mechanisms in PEMWE cells that is expected to have a linear correlation with the applied current density. Oxygen that is dissolved in the water domains of the PEM could be dragged along with the water phase upon proton movement to the cathode, which was already considered in literature.[9,28,32,33] Trinke et al.[28] have shown with ambient pressure measurements at 70 °C with a N117 membrane an oxygen

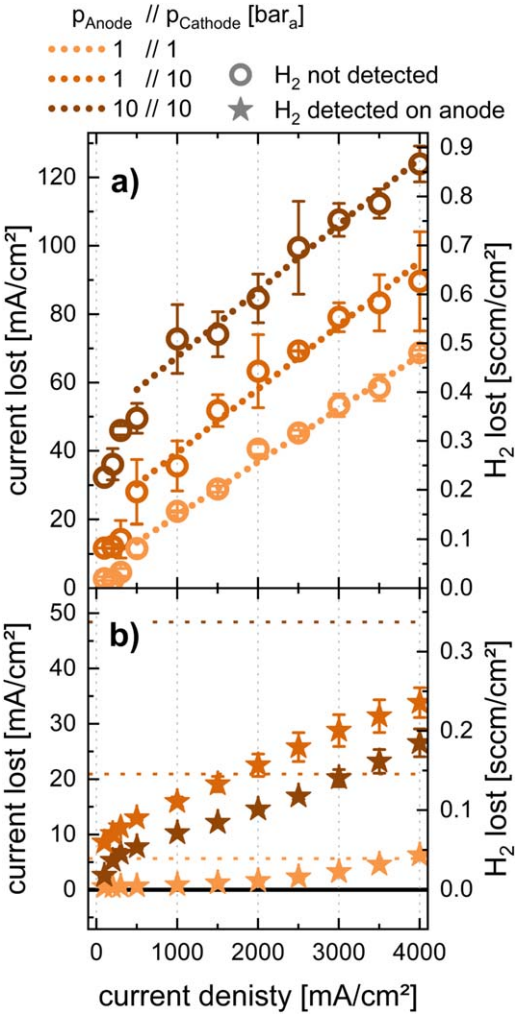

Figure 5. (a) Comparison of the missing hydrogen flux (and corresponding Faradaic current, left axis) over current density at different pressure settings at 80 °C. Light orange corresponds to the measurements at symmetric ambient pressure, orange to the data from the measurements with elevated cathode pressure (differential operation at 1 bar_a/10 bar_a) and dark orange represent the measurements at symmetric elevated pressure of 10 bar_a. The open circles show the data points obtained with their error bars corresponding to the min-max deviation of three independent measurements. A linear fit was applied in the current density of 0.5–4 A cm^{-2} and is shown as dotted lines. (b) Amount of hydrogen flux found on the anode $N_{H_2}^{an}$ as a function of current density and pressure settings. The intercepts of the linear regression of (a) are added here as dotted lines for direct comparison of the relative losses.

content in their Pt-free cathode experiments that also followed a linear behavior with a slope corresponding to roughly $1{\cdot}10^{-8}\ \frac{mol_{O_2}}{A{\cdot}s}$. However, it is not clear whether there unknown Pt-free cathode truly bears insignificant recombination activity.

Looking at the average missing hydrogen flux slope obtained of roughly $0.12\ \frac{sccm_{H_2}}{A}$, this would correspond to an oxygen crossover flux of $0.06\ \frac{sccm_{O_2}}{A}$ or $4.46{\cdot}10^{-8}\ \frac{mol_{O_2}}{A{\cdot}s}$. For an order of magnitude comparison a drag coefficient of $\xi = 4\frac{n_{H_2O}}{n_{H^+}}$ is chosen, which would correspond to a water drag of $4.14{\cdot}10^{-5}\ \frac{mol_{H_2O}}{A{\cdot}s}$. So there would be roughly 10^0 mole of oxygen dragged along for each 10^3 moles of water being dragged, which is a high, but not unreasonable number.

This oxygen crossover mechanism could also be close to back-pressure independent due to the fact that oxygen permeation through the PEM is generally diffusion limited.[11,32] This means that the solubility of oxygen in PEMs is a low barrier for oxygen crossover, no matter whether the transport through the PEM is caused by diffusion or electro-osmotic drag. Minding that the exact solubility coefficients of oxygen in the PEM during water electrolysis conditions are hardly studied and as the activity of oxygen at the electrode/electrolyte interface is unknown, we can not do a deeper sense check at this point. But we want to bring awareness to the community that electro-osmotic drag could indeed largely affect the Faradaic efficiency of PEMWE.

Consequently, we assigned the constant slope of the linear fit to the missing gas flux to be caused by recombination at the cathode of the dragged along oxygen with the hydrogen present. The y-intercept is the parameter leading to the different absolute amounts of missing gas fluxes for the different pressure cases. These intercept values are added to Fig. 5b as dotted lines for comparison. As clearly visible, this intercept is dependent on both, the backpressure on the cathode (light orange vs orange line) and the backpressure on the anode (orange vs dark orange line). An increase in gas crossover flux with partial pressure increase is generally expected.

Comparing the ambient pressure results with the results from the differential pressure measurements at 1 bar_a/10 bar_a, we would assume the difference to not be caused by a change in oxygen crossover as the anode operation conditions were not changed. We hypothesize that the higher amount of missing gases in the latter case stems from an increased hydrogen crossover flux that is, however, not leaving the anode compartment of the PEMWE cell. The iridium oxide anode catalyst must therewith have an HOR activity that is high enough to reduce the Faradaic current used for the OER but low enough to still allow significant amounts of hydrogen being able to leave the cell and be detected by the MS as apparent hydrogen crossover $N_{H_2}^{an}$.

An increase in cathode backpressure by 9 bar resulted in an increase in current density independent missing gas flux from $0.04\ \frac{sccm_{H_2}}{cm^2}$ to $0.15\ \frac{sccm_{H_2}}{cm^2}$. At the same time, the amount of hydrogen detected in the anode exhaust increases as well (Fig. 5b). The latter follows a simple pressure dependent increase according to the partial pressure of hydrogen on the cathode (i.e., a factor of roughly 18) up to a current density of 1.5 A cm^{-2}. At higher current densities the exponential increase observed for the ambient pressure measurements decreases this ratio down to only a factor of 5.4 at a current density of 4 A cm^{-2}. Assuming our hypothesis to be correct and that the increase in missing hydrogen flux upon pressure increase at the cathode really stems from an increase in HOR current at the anode, a deeper understanding of the HOR activity of the catalyst under PEMWE operation would be necessary. Just as the exponential increase of hydrogen content at the anode upon current density increase during ambient pressure operation still lacks a mechanistic understanding, we can only try to explain the data based on basic hypotheses without being able to physically explain the quantities observed.

Hartig-Weiss et al.[34] have shown the implementation of a Pt-wire micro-reference electrode into a running PEMWE cell with two N212 membranes stacked to form the PEM. They have observed the potential of the reference electrode to undergo a distinct jump from close to 0 V vs the cathode up to 1 V vs the cathode when the current density exceeded 2.1 A cm^{-2} for a PEMWE cell operated at 1 bar_a/10 bar_a differential operation. This jump can be explained by a change in atmosphere surrounding the Pt-wire micro-reference from hydrogen-rich to oxygen-rich. We have hypothesized the intercept of the linear fit of the missing gas flux to actually represent an additional hydrogen flux to the anode. Adding this $0.15\ \frac{sccm_{H_2}}{cm^2}$ flux to the amount of hydrogen actually detected at the anode $N_{H_2}^{an}$ would therewith represent the true hydrogen crossover. At a current density of 2.5 A cm^{-2} the hydrogen flux for the 1 bar_a/10 bar_a differential operation would correspond to $0.33\ \frac{sccm_{H_2}}{cm^2}$. The linear slope of the

missing gas flux that we had assigned to the oxygen crossover would represent an oxygen flux of 0.16 $\frac{sccm_{O_2}}{cm^2}$, i.e., the atmosphere would change at this current density from hydrogen-rich to oxygen-rich (taking into account the 2:1 ratio of hydrogen and oxygen[35]). Our results and hypotheses therewith (semi-)quantitatively fit the measurements of the micro-reference electrode shown by Hartig-Weiss et al.[34]

Comparing the 1 bar_a/10 bar_a differential pressure measurements with the symmetric elevated pressure results obtained from the 10 bar_a/10 bar_a measurements, the current density independent missing gas flux increases from 0.15 $\frac{sccm_{H_2}}{cm^2}$ to 0.34 $\frac{sccm_{H_2}}{cm^2}$, almost twice the increase observed for the cathode pressure elevation. Another important finding that has to be discussed along this observation is the amount of the apparent hydrogen crossover $N_{H_2}^{an}$. It is decreased by $0.03 - 0.06 \frac{sccm_{H_2}}{cm^2}$ upon increase of the anode backpressure for all analyzed current densities.

Revisiting Fig. 1 we have introduced the term apparent hydrogen crossover for $N_{H_2}^{an}$ because it might differ from the actual hydrogen crossover $N_{H_2}^{cross}$ if the anode bears a finite HOR activity. A decrease in $N_{H_2}^{an}$ could therewith be caused either by (i) a decrease in the source term $N_{H_2}^{cross}$ or by (ii) an increase in the sink term $N_{H_2}^{HOR}$ (see also right hand side of Fig. 1). Hypotheses on how they could be affected by an increase in anode backpressure are discussed in the following. (i-a) The amount of oxygen crossing over to the cathode could deplete hydrogen at the cathode/electrolyte interface upon recombination forming water and therewith change the source term for the hydrogen crossover to the anode compartment. (i-b) The coverage of gas and water at the anode/electrolyte interface is changing with the backpressure at the anode, altering the volatility of the dissolved hydrogen from the electrolyte into the anode compartment. (ii-a) The same amount of hydrogen reaches the anode but a larger share of it is undergoing HOR instead of reaching the anode exhaust. This could be possible due to the fact that at elevated anode pressure the retention time of the oxygen product gas (and therefore the crossover hydrogen gas) is increased due to the lower volumetric evolution rate. (ii-b) In principle, also the HOR activity of the catalyst could change upon change of the backpressure on the anode due to the different surface potential of the catalyst caused by the high activity of oxygen. All mechanisms would at the same time lead to an increase in current density independent missing gas flux, which is observed as well. Of course, a combination of those mechanisms is just as likely.

It becomes evident that the gas crossover quantities and the share of hydrogen flux at the cathode are not straight forward to quantitatively assign to different possible loss terms. By running three independent MEAs under the afore described pressure conditions we are confident that the results obtained are true. We wanted to focus on the phenomenological description of the results obtained and tried not to draw conclusions by favoring one mechanism over the multitude of other possible explanations. However, we want to stress the most important findings of our product gas analysis:

- Oxygen crossover is a so far hardly studied phenomenon in PEMWE but might have a significant impact on the overall amount of hydrogen that can be attained.
- The apparent hydrogen flux observed at the anode is not a good descriptor regarding the overall amount of hydrogen lost.
- Gas crossover in PEMWE during operation is not just simple permeation that can be estimated based on the pure material coefficients such as solubility, diffusivity and volatility obtained during steady state *in situ* measurements.
- Many aspects that will alter the gas crossover behavior are not well understood, which makes comparison of crossover data from different studies especially difficult.
- The anode catalyst, its mutable surface chemistry, the electrodes' structures, the nature of the electrode/electrolyte interfaces as well as the flow conditions through the electrodes can all affect the hydrogen flux exiting the cathode and therewith the hydrogen production efficiency. Neither of them is truly understood and some basic understanding is still missing.

Besides all of those open ends, we want to show how the described phenomena and experimentally determined gas flux quantities actually affect the hydrogen production efficiency.

Change of the hydrogen Faradaic efficiency with operation conditions.—After thoroughly studying the gas fluxes attained from the PEMWE cells, the actual Faradaic efficiencies for hydrogen production as a function of current density and operating pressures are compared.

The most important information in Fig. 6 is depicted as green bars. Those represent the amount of hydrogen quantified in the

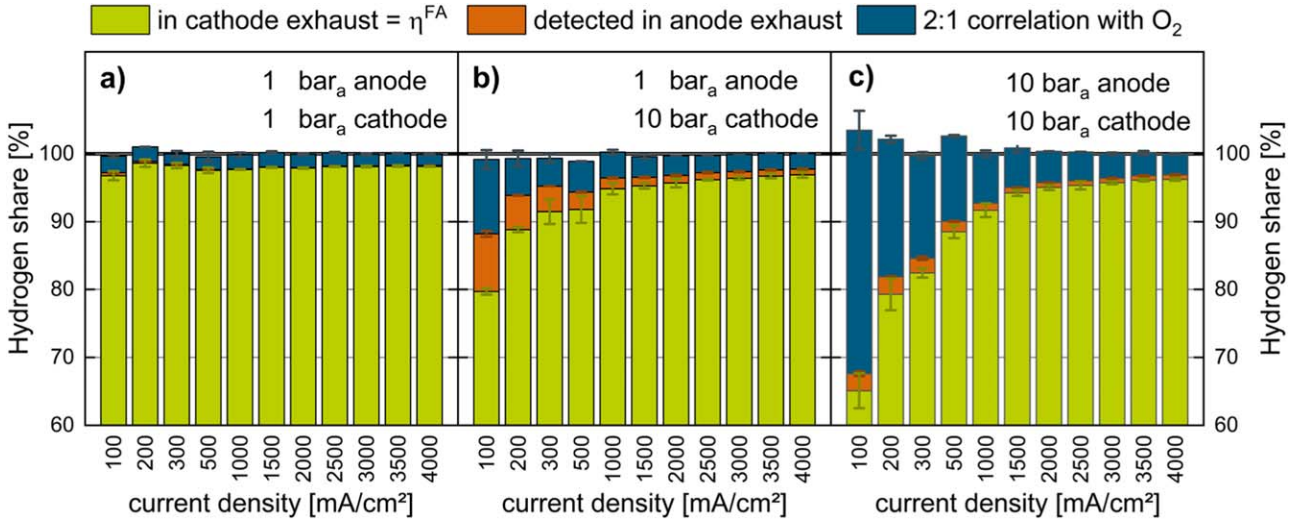

Figure 6. Distribution of hydrogen flux share for the PEMWE single cells based on a N212 membrane running with 20 ml min^{-1} of H_2O supply to the anode at 80 °C for the current density range of 0.1–4 A cm^{-2}. The share of hydrogen found in the cathode exhaust (i.e., the Faradaic efficiency) is shown in green bars (starting at 0). The apparent hydrogen crossover is stacked in orange bars. Closing the hydrogen balance is possible by using the amount of oxygen missing in the overall gas balance and taking into account the 2:1 correlation of hydrogen and oxygen produced (stacked blue bars). The shown bar charts represent the measurements executed at (a) symmetric ambient pressure, (b) differential operation with 10 bar_a cathode backpressure and (c) at symmetric elevated backpressure of 10 bar_a. Error bars are based on the min-max deviation of the three independently measured MEAs.

cathode exhaust at different current densities for the three studied pressure cases. This is the actual Faradaic efficiency of the PEMWE cells, minding that hydrogen is the goal product. For the ambient pressure operation shown in Fig. 6a, the Faradaic efficiency of the cell is almost independent of the current density operated at, being in the range of 97.5 ± 0.7%. The amount of hydrogen detected in the anode exhaust is added as orange bars and is almost invisible for the atmospheric pressure operation. In Fig. 5 we have discussed the amount of missing hydrogen, i.e., the difference between the amount theoretically produced based on Faraday's Law (100%) and the sum of hydrogen found in both exhausts. To show once more, that the amount of missing oxygen can just as well be used to quantify the amount of missing hydrogen, it is stacked to the bars representing the hydrogen share found in the anode and in the cathode as dark blue bars in the known 2:1 ratio. Therewith the hydrogen mass balance can be closed with the average values of the three different hydrogen shares adding up to 100% for all current densities.

The linear dependency of the amount of missing gas at current densities exceeding 0.5 A cm^{-2} can also be seen in Fig. 6 as a close to constant loss in Faradaic efficiency depicted as blue bars. The change in intercept for the elevated pressure cases leads to a small distortion of course.

Increasing the cathode backpressure in Fig. 6b the Faradaic efficiency loss caused by the hydrogen crossover is increased as depicted by the significant share of the orange bars as well as the increase of the missing gas share represented by the blue bars (based on the oxygen mass balance). We want to stress once more that the Faradaic loss by the hydrogen crossover is most likely bigger than the apparent hydrogen crossover $N_{H_2}^{an}$. The actual Faradaic efficiency of the PEMWE cells increases with current density for the 1 bar_a/10 bar_a operation from only 79.7% at 0.1 A cm^{-2} up to 96.9% at 4 A cm^{-2}. This is caused by both, a decrease in hydrogen share loss observed at the anode and a relative decrease of missing gas flux with current density.

The anode backpressure was increased in the last pressure variation as well for analytical reasons even though a PEMWE cell would most likely not be chosen to operate like this. Here the Faradaic efficiency changes the strongest over current density from 65.1% up to 96.2% when increasing the current density from 0.1 A cm^{-2} to 4 A cm^{-2} (green bars in Fig. 6c). Interestingly, here the loss that can be directly assigned to the share of hydrogen found in the anode exhaust is lower compared to the differential pressure operation at 1 bar_a/10 bar_a, which was already discussed along Fig. 5.

True hydrogen production efficiency of PEMWE single cells.— After thorough analysis of the Faradaic efficiency of the PEMWE single cells, we are now able to do a cell-based hydrogen production efficiency comparison for the different operation conditions.

The top panel in Fig. 7 shows the polarization characteristics of the PEMWE single cells at the different pressure conditions. Upon increase in cathode pressure (triangles vs squares), there is a significant change in reversible cell voltage (45 mV for 10 bar_a cathode backpressure) as already described in literature. The higher cell voltage observed throughout the polarization curve corresponds to an increase of 42–66 mV, which is fairly close to the theoretical predicted change based on the Nernst equation. When adding backpressure to the anode, the observed reversible voltage and kinetic region is hardly changed but a small decrease in overpotential at higher current densities can be observed compared to the differential pressure operation (diamonds vs triangles). This change is not caused by a change in HFR but is assumed to stem from a change in the mass transport resistance at the anode at elevated backpressure.[15]

With representative electrochemistry being obtained at all shown pressure cases, the hydrogen content in the anode exhaust is further analyzed with respect to possible safety concerns arising from formation of explosive mixtures upon hydrogen crossover. The values are shown in the bottom panel of Fig. 7 using the respective symbols. We differentiate two different hydrogen in oxygen contents: As open symbols, we show the hydrogen in oxygen content with the oxygen flux taken from Faraday's Law. Many studies only quantify the hydrogen flux at the anode without quantification of the true oxygen flux.[10,21,24,25,30] By having analyzed the absolute oxygen flux leaving the anode compartment, we can calculate the true hydrogen in oxygen content, which is denoted as closed symbols. This value would correspond to the reading from a H_2 in O_2 safety sensor. For the ambient pressure case (squares), there is hardly any observable difference between the two hydrogen content calculations because the amount of missing gas is rather small (see also Fig. 6). Only at small current densities of less than 100 mA cm^{-2} the quantification of the true oxygen flux actually makes a difference and increases the hydrogen in oxygen share. For all current densities exceeding 30 mA cm^{-2}, the hydrogen in oxygen content stays below the threshold of 2%.

When increasing the cathode pressure to 10 bar_a (triangles) the hydrogen in oxygen content is significantly increased. Only at current densities exceeding 2.5 A cm^{-2} a safe operation can be ensured. Due to the higher loss of oxygen for this operating condition, the difference between the hydrogen in oxygen content assuming 100% Faradaic efficiency for oxygen evolution and the truly measured hydrogen in oxygen content is more pronounced.

For the symmetric operation at elevated pressures of 10 bar_a/10 bar_a (diamonds), hydrogen in oxygen contents of less than 2% are achieved at current densities exceeding 1 A cm^{-2} caused by the lower hydrogen gas flux observed on the anode for this case as shown in Fig. 5b. Due to the higher amount of missing gases, the hydrogen in oxygen content calculated by the two afore described methods differs the most, accounting for almost 0.5% at 0.5 A cm^{-2}. It is therefore important to quantify the true hydrogen in oxygen content rather than only

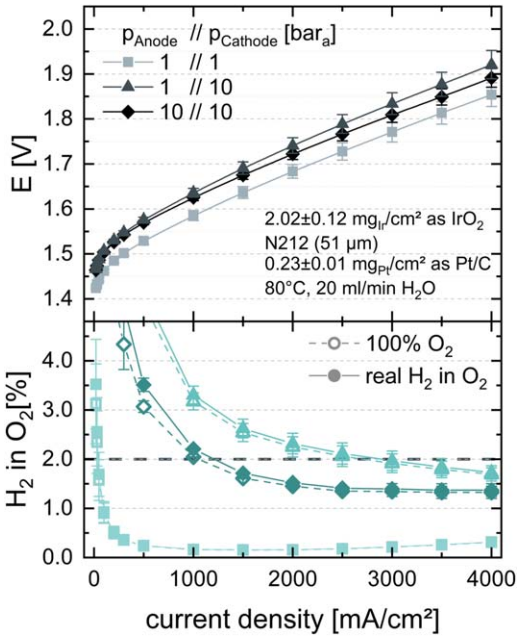

Figure 7. Top: Comparison of polarization curves obtained for the three different pressure cases during the crossover measurement. Bottom: H_2 in O_2 content on the anode over current density. Two different values are shown with open symbols representing the H_2 flux in the anode exhaust normalized by a theoretical production rate of O_2 according to Faraday's Law and closed symbols representing the H_2 flux normalized by the actual O_2 flux found in the anode exhaust. The safety limit of 2% H_2 in O_2 is added as a dashed line. Squares show the data obtained for the ambient pressure case, triangles correspond to the 1 bar_a/10 bar_a operation and diamonds represent the symmetric elevated pressure operation case. Lines between data points are merely added as a guide to the eye.

looking at the hydrogen flux exiting the anode in order to judge safe operation of the PEMWE cells.

Now that the safe operation windows for the different pressure conditions are fixed, the actual hydrogen production efficiency is discussed. For this we multiply the electrical efficiency and the Faradaic efficiency as discussed in the experimental part. The results are shown in Fig. 8. The top panel shows the partial efficiencies, i.e., the electrical efficiency $\eta_{H_2}^{EC}$ (grey shades) and the Faradaic efficiencies $\eta_{H_2}^{FA}$ (green shades).

The highest Faradaic and electrical efficiency is observed for the symmetric ambient pressure case, which is expected due to the lower driving force for gas loss and the lower reversible potential for the gas evolution reactions. The Faradaic efficiency and electrical efficiency for the pressurized cases have already been discussed in Figs. 6 and 7, respectively. Not taking into account the true Faradaic efficiency for hydrogen production—that cannot be quantified based on the pure hydrogen in oxygen flux that is easy to determine experimentally—one would only use the electrical efficiency $\eta_{H_2}^{EC}$ behavior and compare it to the LHV of hydrogen. A common goal is hydrogen production efficiencies exceeding $70\%_{LHV}$, which would correspond to a maximum current density of roughly 3.2 A cm^{-2} for the ambient pressure case, 2.5 A cm^{-2} for the symmetric elevated pressure operation and roughly 2.3 A cm^{-2} for the differential pressure operation at 1 bar_a/10 bar_a based on the electrical efficiency.

When taking into account the real Faradaic efficiency of the system, the overall production efficiency can be calculated and is displayed in the bottom panel of Fig. 8. Also here, the $70\%_{LHV}$ efficiency value is added as a guideline. Additionally, current densities that cannot be aimed for because they exceed the 50% LEL H_2 in O_2 values (see Fig. 7) are only shown as semi-transparent symbols. The results from this analysis are the final window assignment for safe and efficient hydrogen production on those PEMWE single cells.

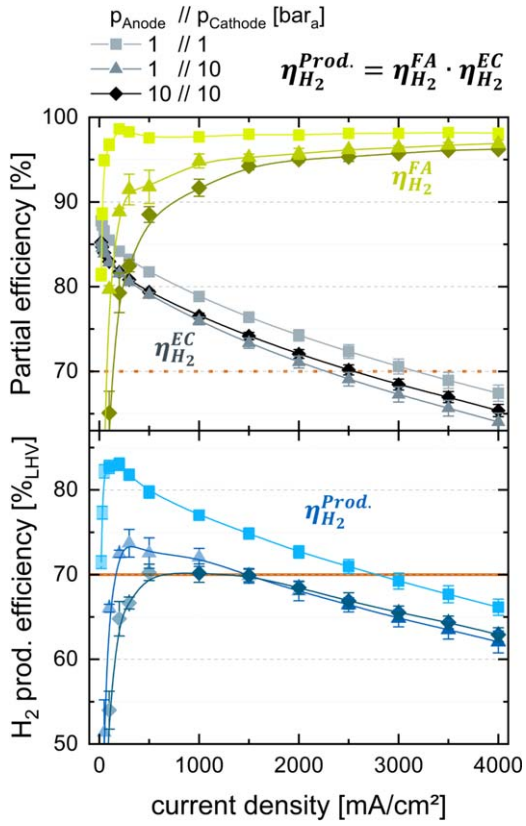

Figure 8. Top: Electrical efficiency (grey shades) and Faradaic efficiency (green shades) over current density for the three studied operating pressure cases. Bottom: Hydrogen production efficiency based on the LHV of the hydrogen gas product. For current densities where the 2% H_2 in O_2 limit is exceeded, the symbols are shown semi-transparent. The reference of $70\%_{LHV}$ is given as an orange line. Squares show the data obtained for the ambient pressure case, triangles correspond to the 1 bar_a/10 bar_a operation and diamonds represent the symmetric elevated pressure operation case. Lines between data points are merely added as a guide to the eye.

In general, at low current densities the possible formation of explosive mixtures is limiting the operation window, whereas the high potentials at high current densities cause the production efficiency to drop below a reasonable value. For the ambient pressure case (light blue squares in bottom panel of Fig. 8), operation between 50 mA cm^{-2} and 2.5 A cm^{-2} is possible. For the differential pressure operation, there is only a very narrow window between 0.2 A cm^{-2} and 1 A cm^{-2} where the production efficiency is above $70\%_{LHV}$. This window is, however, also not possible to operate at due to the hydrogen in oxygen content being above 2%. Though the latter is less of a problem for the symmetric elevated pressure operation, the production efficiency is significantly worse due to the lower Faradaic efficiency, limiting the operating window to a single operating point around a current density of 1 A cm^{-2} that just barely allows operation from a safety point of view.

Conclusions

In this study, we have shown that closing the hydrogen and oxygen mass balance for PEMWE single cells is possible even with small active area lab cells. The amount of missing gas fluxes in the exhaust streams follows the 1:2 ratio of oxygen and hydrogen. We have shown that the amount of missing hydrogen gas easily exceeds the commonly reported hydrogen in oxygen content. By changing the operating pressure of the cell, we were able to show the similar current density dependent deficiency of product gases in the exhaust that follows a linear trend, which might therefore be assigned to oxygen crossover to the cathode caused by the electro-osmotic drag. Additionally, the amount of hydrogen observed in the anode compartment seems not be a good descriptor of the actual hydrogen loss to the anode due to possible HOR activity of the iridium-based anode catalyst. We have therefore introduced the term apparent hydrogen crossover, which is the amount of hydrogen that actually can be quantified at the anode exhaust. By determining the true Faradaic efficiency with respect to hydrogen production, we showed that gas crossover phenomena in the cell significantly diminish the efficient operation window for PEMWE.

Despite being able to phenomenologically describe the change in Faradaic efficiency of the product gases with current density and pressure, we were only able to offer several hypotheses for those dependencies. It became evident that there is still a lack of fundamental understanding of PEMWE processes. Membrane creep might be an important factor to consider when evaluation the system efficiency with thin, non-reinforced membranes especially over the systems lifetime.

A major unknown is the nature of the electrode/electrolyte interface at both, the anode and cathode. While steady state gas permeation through PEM has been studied extensively, the results of this study show that gas crossover in operating PEMWE is by far more complex. Thorough studies on the electrodes' structures, the nature of the electrode/electrolyte interfaces as well as the flow conditions through the electrodes with respect to their effect on the product gas fluxes are still missing and will be necessary to bring the most efficient configuration and systems into application.

Acknowledgments

The authors gratefully acknowledge the financial support of this work by the Federal Ministry of Economic Affairs and Climate Action in Germany within the project HoKaWe (grant number 03EI3029A). We thank Umicore AG & Co. KG, PMC—FC for providing the electrocatalysts for this study.

ORCID

Anna T. S. Freiberg https://orcid.org/0000-0002-7885-7632
Simon Thiele https://orcid.org/0000-0002-4248-2752

References

1. Z. Taie, X. Peng, D. Kulkarni, I. V. Zenyuk, A. Z. Weber, C. Hagen, and N. Danilovic, *ACS Appl. Mater. Interfaces*, **12**, 52701 (2020).
2. M. Clapp, C. M. Zalitis, and M. Ryan, *Catal. Today*, **420** (2023).
3. K. Bareiß, C. de la Rua, M. Möckl, and T. Hamacher, *Appl. Energy*, **237**, 862 (2019).
4. J. Hemauer, S. Rehfeldt, H. Klein, and A. Peschel, *Int. J. Hydrogen Energy*, **48**, 25619 (2023).
5. M. Carmo, G. P. Keeley, D. Holtz, T. Grube, M. Robinius, M. Müller, and D. Stolten, *Int. J. Hydrogen Energy*, **44**, 3450 (2019).
6. M. Carmo, D. L. Fritz, J. Mergel, and D. Stolten, *Int. J. Hydrogen Energy*, **38**, 4901 (2013).
7. S. M. Saba, M. Müller, M. Robinius, and D. Stolten, *Int. J. Hydrogen Energy*, **43**, 1209 (2018).
8. V. Schröder, B. Emonts, H. Janßen, and H. P. Schulze, *Chem. Eng. Technol.*, **27**, 847 (2004).
9. M. Schalenbach, M. Carmo, D. L. Fritz, J. Mergel, and D. Stolten, *Int. J. Hydrogen Energy*, **38**, 14921 (2013).
10. M. Bernt, J. Schröter, M. Möckl, and H. A. Gasteiger, *J. Electrochem. Soc.*, **167**, 124502 (2020).
11. X. Luo, G. Lau, M. Tesfaye, C. R. Arthurs, I. Cordova, C. Wang, M. Yandrasits, and A. Kusoglu, *J. Electrochem. Soc.*, **168**, 104517 (2021).
12. M. Schalenbach, T. Hoefner, P. Paciok, M. Carmo, W. Lueke, and D. Stolten, *The Journal of Physical Chemistry C*, **119**, 25145 (2015).
13. A. Stähler, M. Stähler, F. Scheepers, W. Lehnert, and M. Carmo, *J. Electrochem. Soc.*, **169**, 034522 (2022).
14. P. Trinke, P. Haug, J. Brauns, B. Bensmann, R. Hanke-Rauschenbach, and T. Turek, *J. Electrochem. Soc.*, **165**, F502 (2018).
15. S. A. Grigoriev, P. Millet, S. V. Korobtsev, V. I. Porembskiy, M. Pepic, C. Etievant, C. Puyenchet, and V. N. Fateev, *Int. J. Hydrogen Energy*, **34**, 5986 (2009).
16. H. Ito, N. Miyazaki, M. Ishida, and A. Nakano, *Int. J. Hydrogen Energy*, **41**, 20439 (2016).
17. M. Bernt, C. Schramm, J. Schröter, C. Gebauer, J. Byrknes, C. Eickes, and H. A. Gasteiger, *J. Electrochem. Soc.*, **168**, 084513 (2021).
18. T. Srour et al., *Int. J. Hydrogen Energy*, **58**, 351 (2024).
19. T. Schuler, C. C. Weber, J. A. Wrubel, L. Gubler, B. Pivovar, F. N. Büchi, and G. Bender, *Adv. Ener. Mat.*, **14**, 2302786 (2024).
20. C. Klose, P. Trinke, T. Böhm, B. Bensmann, S. Vierrath, R. Hanke-Rauschenbach, and S. Thiele, *J. Electrochem. Soc.*, **165**, F1271 (2018).
21. D. Abbas, A. Martin, P. Trinke, M. Bierling, B. Bensmann, S. Thiele, R. Hanke-Rauschenbach, and T. Böhm, *J. Electrochem. Soc.*, **169**, 124514 (2022).
22. S. Garbe, U. Babic, E. Nilsson, T. J. Schmidt, and L. Gubler, *J. Electrochem. Soc.*, **166**, F873 (2019).
23. S. Garbe, J. Futter, T. J. Schmidt, and L. Gubler, *Electrochim. Acta*, **377**, 138046 (2021).
24. Z. Zhang, Z. Han, A. Testino, and L. Gubler, *J. Electrochem. Soc.*, **169**, 104501 (2022).
25. Z. Zhang, A. Baudy, A. Testino, and L. Gubler, *ACS Appl. Mater. Interfaces*, **16**, 23265 (2024).
26. M. Schalenbach and D. Stolten, *Electrochim. Acta*, **156**, 321 (2015).
27. P. Trinke, B. Bensmann, and R. Hanke-Rauschenbach, *Int. J. Hydrogen Energy*, **42**, 14355 (2017).
28. P. Trinke, B. Bensmann, and R. Hanke-Rauschenbach, *Electrochem. Commun.*, **82**, 98 (2017).
29. M. Bernt and H. A. Gasteiger, *J. Electrochem. Soc.*, **163**, F3179 (2016).
30. A. Martin, P. Trinke, B. Bensmann, and R. Hanke-Rauschenbach, *J. Electrochem. Soc.*, **169**, 094507 (2022).
31. A. Weiß, A. Siebel, M. Bernt, T. H. Shen, V. Tileli, and H. A. Gasteiger, *J. Electrochem. Soc.*, **166**, F487 (2019).
32. S. A. Grigoriev, A. A. Kalinnikov, P. Millet, V. I. Porembsky, and V. N. Fateev, *J. Appl. Electrochem.*, **40**, 921 (2009).
33. S. Fahr, F. K. Engel, S. Rehfeldt, A. Peschel, and H. Klein, *Int. J. Hydrogen Energy*, **68**, 705 (2024).
34. A. Hartig-Weiß, M. Bernt, A. Siebel, and H. A. Gasteiger, *J. Electrochem. Soc.*, **168** (2021).
35. S. Takaichi, H. Uchida, and M. Watanabe, *Electrochem. Commun.*, **9**, 1975 (2007).